Energy & Environmental Science

RSC Publishing

PAPER

View Article Online
View Journal

Cite this: DOI: 10.1039/c3ee40453f

An analysis of the optimal band gaps of light absorbers in integrated tandem photoelectrochemical water-splitting systems†

Shu Hu,[ae] Chengxiang Xiang,[ae] Sophia Haussener,[bd] Alan D. Berger[cd] and Nathan S. Lewis*[ae]

The solar-to-hydrogen (STH) efficiency limits, along with the maximum efficiency values and the corresponding optimal band gap combinations, have been evaluated for various combinations of light absorbers arranged in a tandem configuration in realistic, operational water-splitting prototypes. To perform the evaluation, a current–voltage model was employed, with the light absorbers, electrocatalysts, solution electrolyte, and membranes coupled in series, and with the directions of optical absorption, carrier transport, electron transfer and ionic transport in parallel. The current density *vs.* voltage characteristics of the light absorbers were determined by detailed-balance calculations that accounted for the Shockley–Queisser limit on the photovoltage of each absorber. The maximum STH efficiency for an integrated photoelectrochemical system was found to be ~31.1% at 1 Sun (=1 kW m^{-2}, air mass 1.5), fundamentally limited by a matching photocurrent density of 25.3 mA cm^{-2} produced by the light absorbers. Choices of electrocatalysts, as well as the fill factors of the light absorbers and the Ohmic resistance of the solution electrolyte also play key roles in determining the maximum STH efficiency and the corresponding optimal tandem band gap combination. Pairing 1.6–1.8 eV band gap semiconductors with Si in a tandem structure produces promising light absorbers for water splitting, with theoretical STH efficiency limits of >25%.

Received 7th February 2013
Accepted 11th April 2013

DOI: 10.1039/c3ee40453f

www.rsc.org/ees

Broader context

An integrated system that allows for the direct production of fuels from sunlight would provide a scalable, sustainable source of clean fuels for grid storage as well as for use in the transportation sector. Because all of the components of such a complete system must operate under mutually compatible conditions, an assessment of the required materials properties necessitates a systems-level analysis of the operational conditions of an integrated solar-fuel generator. Accordingly, the optimal system efficiency has been calculated for various solar-fuel generator system geometries and component dimensions, as a function of the band gaps of the light absorber components that serve to capture and convert sunlight into chemical fuels. Dual band gap light absorber configurations have been evaluated, with the dual band gap, tandem structure, providing optimal efficiency and thus a preferred approach, to effect direct solar-fuel production. The assessment has incorporated a variety of systems-level parameters that are present in an actual operating solar-fuel generator system, including the thermodynamic constraints on the light absorbers as given by the Shockley–Queisser detailed-balance limit, the overpotentials of earth-abundant catalysts for water oxidation and reduction reactions, and the effects of solution resistance and light absorber quality on the overall conversion process of sunlight into chemical fuels.

I Introduction

An integrated photoelectrochemical (PEC) system containing light absorbers, electrocatalysts for the hydrogen-evolution reaction (HER) and for the oxygen-evolution reaction (OER), electrolytes, and membranes has the potential to achieve the high-efficiency production of fuels from sunlight, particularly photoelectrolysis of water to generate hydrogen (H_2) and oxygen (O_2) renewably:

In acidic conditions:

$$4H^+ + 4e^- \rightarrow 2H_2$$

$$2H_2O \rightarrow O_2 + 4H^+ + 4e^-$$

[a]Division of Chemistry and Chemical Engineering, 210 Noyes Laboratory, California Institute of Technology, Pasadena, CA, 91125, USA. E-mail: nslewis@caltech.edu

[b]Institute of Mechanical Engineering, Ecole Polytechnique Federale de Lausanne, 1015 Lausanne, Switzerland

[c]Department of Chemical and Biomolecular Engineering, University of California, 201 Gilman Hall, Berkeley, CA 94720, USA

[d]Joint Center for Artificial Photosynthesis, Lawrence Berkeley National Laboratory, Berkeley, CA 94720, USA

[e]Joint Center for Artificial Photosynthesis, California Institute of Technology, 1200 E. California Blvd., Pasadena, CA, 91125, USA

† Electronic supplementary information (ESI) available: Detailed-balance calculations for the current–voltage properties of the light absorbers. See DOI: 10.1039/c3ee40453f

In alkaline conditions:

$$4H_2O + 4e^- \rightarrow 2H_2 + 4OH^-$$

$$4OH^- \rightarrow O_2 + 4H_2O + 4e^-$$

To date, various integrated PEC systems and key photoactive PEC components have been proposed and demonstrated experimentally. Systems based on single light-absorber components have been proposed, but their solar-to-hydrogen (STH) efficiencies will be low, despite the use of single-crystal semiconductors, due to the low optical absorption of the light absorber component of such a system.[1–3] Photochemical diodes[4,5] featuring a bi-component light absorber of opposite doping types were described in the 1970s. Similarly, bi-component particulate or particle-molecular dye photosystems have been suggested for use in spontaneous water splitting under visible-light illumination using a suitable redox mediator.[6–9] However, a membrane that is selective to the redox mediator is necessary, because the evolved H_2 and O_2 should be separated by the membrane for safety considerations. Additionally, undesirable back-reactions, *e.g.* recombination of evolved gas with redox mediators, or recombination of evolved gas with photogenerated carriers under illumination, need to be minimized.

These studies concur with the premise that a tandem PEC system that contains a two-component or two-junction light absorber is needed to realize water splitting with high STH efficiencies. Such a tandem approach is analogous to the *Z*-scheme of natural photosynthesis.[10] By using light-absorbing materials (either inorganic semiconductors or organic dye-molecules) with complementary absorption spectra, a two-component photosystem[8,9] or a two-junction PEC system can effectively capture various portions of the solar spectrum, providing the photovoltage needed to split water. However, the STH efficiency depends on both the photovoltage and the photocurrent density of the light absorber, and the maximum photocurrent density decreases with an increasing number of junctions. Despite this, the STH efficiencies of a two-junction PEC system greatly outperform that of a single-junction system.[11] Two-junction PEC photoelectrodes or prototype water-splitting systems using inorganic semiconductors such as InGaP/GaAs,[12] AlGaAs/Si,[13] and InGaP/InGaAs[14] combinations have achieved the STH efficiencies of 10–20%. Triple-junction amorphous Si (a-Si:H) solar cells have also served as light absorber components to electrolyze water with earth-abundant catalysts.[15,16]

Modeling efforts on full system prototypes have identified and quantified the important design criteria required for an integrated solar-driven water-splitting system to achieve an optimal STH efficiency.[17] The rational design of such an integrated PEC system requires consideration of the interplay among several key components: (1) a tandem light absorber component for maximizing the photocurrent densities while providing sufficient photovoltage to drive the water-splitting reactions; (2) an ion-selective membrane, for providing acceptably low rates of recombination of H_2 and O_2 thereby avoiding generation of an explosive gas mixture and simultaneously minimizing Ohmic losses across the membrane; (3) a device architecture for minimization of ion transport losses in the liquid electrolyte. This particular study has also shown that design optimization of integrated PEC systems may allow for spatial placement of the electrocatalysts to minimize their "parasitic" optical absorption.[17]

Recently, both experimental and modeling efforts have extended the theoretical framework advanced by Bolton *et al.*[11] and Nozik,[4,5] and have suggested that the operating point of the PEC system can be determined from the separately measured properties of the light absorbers in conjunction with the properties of the electrochemical loads that include the kinetics of HER and OER electrocatalysts and any solution resistances in the system.[14,15,18–20] The operating photovoltage produced by the light absorbers should exceed the sum of the thermodynamically required potential difference, the resistance losses of the electrolytes, and any overpotentials that are required to drive water splitting at a given current density. When the photovoltage constraint is met, the operating photocurrent density in an integrated PEC system therefore determines the STH efficiency.

In this study, the STH efficiency limits in an integrated PEC system are evaluated, with the primary focus on the maximum STH efficiency value of the PEC system and the corresponding optimal band gap combinations of the tandem light absorber. First, the configurations of water-splitting systems and the theoretical considerations of their operation points are discussed. A zero-dimensional (0-D) current–voltage model has been employed, with the light absorbers, electrocatalysts, solution electrolyte, and membranes coupled in series and with the directions of optical absorption, carrier transport, electron transfer and ionic transport in parallel. The simplified model has been used to capture the key physical and chemical nature of prototypical integrated PEC systems, and should thus guide choices of light absorbers for splitting water at maximum efficiencies. This work is complimentary to other ongoing efforts to estimate the maximum practical STH efficiencies subject to an estimate of the practically realizable behavior of an operational PEC system.[20b]

Each component of the PEC system has been numerically modeled to calculate the STH efficiency values for all band gap combinations of interest: for example, the current density–voltage (*J–V*) characteristics of the light-absorbing junctions or components at a given band gap combination has been determined by detailed-balance calculations, with the resulting energy-conversion efficiency known as the Shockley–Queisser limit.[21] The electrochemical load was modeled using literature values for state-of-the-art electrocatalysts and reasonable values for the ion-transport resistance in the system. The maximum STH efficiency possible for an integrated PEC system has been investigated, followed by consideration of additional factors in the system that may further restrict the STH efficiency limits. Finally, we have compared the efficiency of an integrated PEC water-splitting system with that of a system consisting of photovoltaic systems electrically wired to discrete electrolysis units.

II Theory

A Two configurations of water-splitting systems

A1 Photocathode + photoanode PEC. Fig. 1a illustrates the photocathode + photoanode PEC (Configuration A), in which a photocathode and a photoanode are connected back-to-back

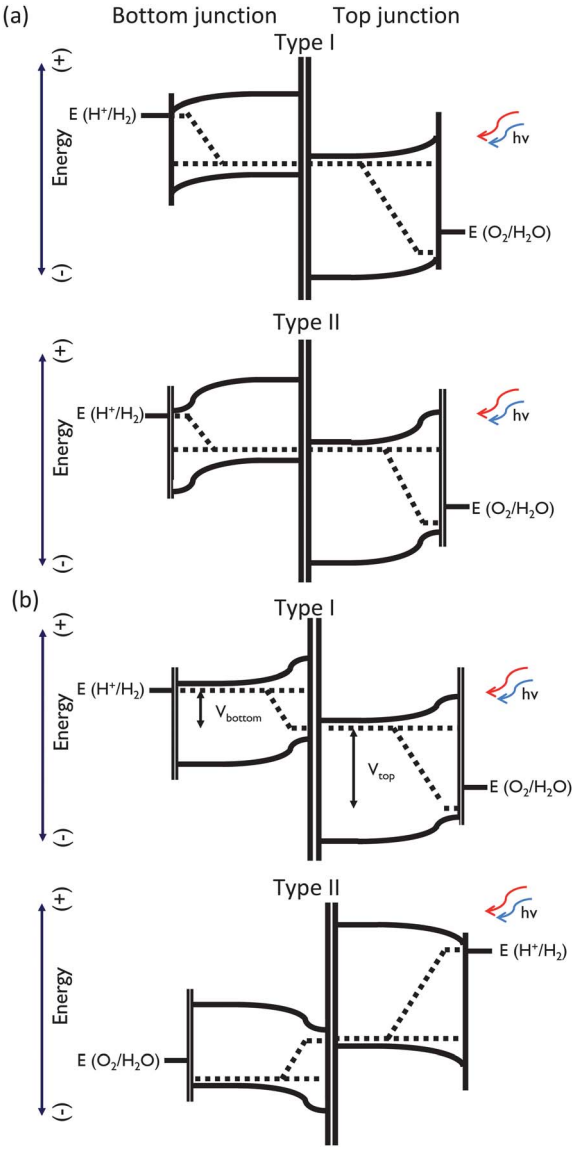

Fig. 1 Schematic energy band diagrams of an integrated photoelectrochemical (PEC) system under 1 Sun illumination for (a) the photocathode + photoanode PEC system, denoted as Configuration A, and (b) the tandem light absorber + electrocatalyst PEC system, denoted as Configuration B. Types I and II illustrate the semiconductor–liquid junctions and buried junctions, respectively, as described in the text.

with an Ohmic contact. The photogenerated minority-carrier electrons drift and diffuse to the photocathode–electrolyte interface and reduce H^+ to H_2, whereas the photogenerated minority-carrier holes drift and diffuse to the photoanode–electrolyte interface and oxidize water to O_2. The majority carriers (holes in the photocathode and electrons in the photoanode) recombine at the Ohmic contact, which is indicated by the doubly thick line that connects both photoelectrodes back-to-back.

The asymmetrical barrier for effective separation of photogenerated carriers in this configuration can either be a semiconductor–liquid junction that is formed at the photoelectrode–electrolyte interface (Fig. 1a, Type I), or a "buried" junction (Fig. 1a, Type II) that is formed inside the photoelectrode. In both cases, the photogenerated minority carriers drift and diffuse in mutually opposite directions to the semiconductor–liquid interfaces.

In the subsequent modeling, the photoanode has been taken to be the wider band gap junction at the top, and the photocathode has been taken to be the narrower band gap at the bottom. However, the doping polarity of the two light-absorbing components can be interchanged, with the top junction being the photocathode and the bottom being the photoanode. Photochemical diodes,[22] dye-sensitized photosystems,[3,8,9] and two-component particulate systems with redox relays (equivalent to an Ohmic contact in terms of a circuit element)[6,7] can be categorized as the photoanode + photocathode PEC system. With minimization of both gas crossover and back reactions, the STH efficiency limit of two-component particulate systems will be comparable to that of photochemical diodes.

A2 Tandem absorber + electrocatalysts PEC. The tandem absorber + electrocatalysts PEC, denoted as Configuration B, consists of a tandem two-junction light absorber as well as HER and OER electrocatalysts that are in electrical connection to the electron and hole collectors of the tandem light absorber, respectively (Fig. 1b). Similar to Configuration A, both junctions can be "buried" (Fig. 1b, Type I) or one of the junctions can be at the semiconductor–liquid interface (Fig. 1b, Type II). The doping polarity of the two junctions can also be interchanged (Fig. 1b, Type II). Relevant examples of the tandem absorber + electrocatalysts PEC configuration include dual-junction GaInP/GaAs photoelectrodes,[12] AlGaAs/Si PEC systems,[13] and triple-junction amorphous Si PEC systems.[15,16]

B Operating principles of integrated water-splitting systems

Fig. 2 shows the operating principles of the photocathode + photoanode PEC, tandem absorber + electrocatalysts PEC, and PV + electrolyzer configurations. For the photocathode + photoanode PEC, the operating point is the intersection (red point in Fig. 2a) between the current density–potential (J–E) curve of the photocathode (green curve in Fig. 2a) and that of the photoanode (blue curve in Fig. 2a).[18] The J–E behavior of each photoelectrode can be separately measured in a photoelectrochemical cell through use of a three-electrode potentiostatic apparatus, and the electrode potentials can be adjusted with respect to the reversible hydrogen electrode (RHE). In our calculations, the photoanode and the photocathode potentials were related to the operating photovoltages of the corresponding junction, V_{top} and V_{bottom}, and the catalyst overpotentials, η_{OER} and η_{HER}, at a photocurrent density, j, with respect to the standard potential of O_2/H_2O and H^+/H_2, respectively:

$$E_{photoanode}(j) = 1.23\ V - V_{top}(j) + \eta_{OER}(j) + jR/2 \quad (1)$$

$$E_{photocathode}(j) = V_{bottom}(j) + \eta_{HER}(j) - jR/2 \quad (2)$$

$\eta_{HER}(j)$ is taken as negative because the HER electrocatalyst is driven cathodically. 1.23 V is the thermodynamic potential difference of O_2/H_2O and H^+/H_2 under standard conditions (25 °C, 1 molar H^+(aq), and 1 atm). $V_{top}(j)$ and $V_{bottom}(j)$ were

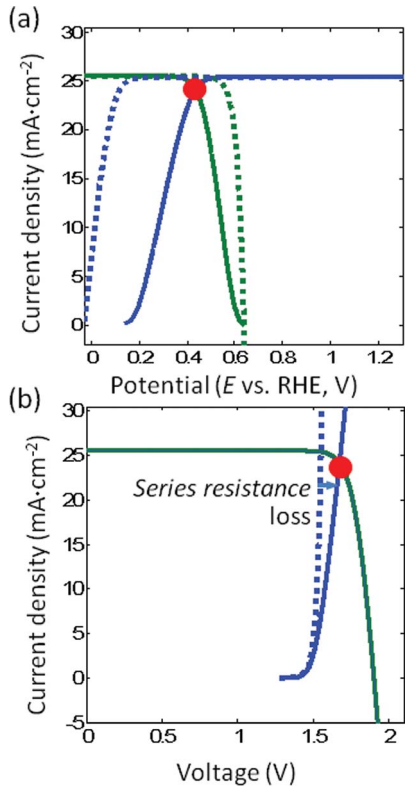

Fig. 2 Operation points (red dots) of (a) a photocathode + photoanode PEC configuration, and (b) a tandem absorber + electrocatalyst PEC configuration. The dashed blue and green curves in (a) are the ideal *J–V* properties of the various photoelectrode materials. The dashed curve in (b) represents the electrochemical load without solution resistance losses. For (a) and (b), Pt and RuO_2 were chosen as the HER and OER catalysts, respectively, the light absorber had FF = 0.85, and the solution resistance was 5 ohm cm^{-2}.

modeled considering the Shockley–Queisser limit. The sum of the current density–voltage (*J–V*) behavior of each junction of the light absorber and the *J–E* behavior of the electrocatalyst is a reasonable approximation to the efficiency limit of photoelectrodes, because in this limit both the light absorber and the electrocatalyst can be considered to operate independently. This limit is possible when: (1) defects are not present at the light absorber–catalyst interfaces; and (2) the barrier height of the light absorber–catalysts–liquid interface in Type I or the buried junction in Type II is close to the band gap. To account for the Ohmic potential drop, a solution resistance of *R*/2 was applied to each photoelectrode, where *R* is the solution resistance per unit area (ohm cm^{-2}, $A = 1\ cm^2$).

The dashed blue and green curves in Fig. 2a are the *J–V* properties of the top and the bottom junctions, respectively, with the solid blue and green curves representing the photoelectrode properties calculated from the dashed curves using eqn (1) and (2). During spontaneous water splitting, the photoanode and the photocathode are connected in series: *i.e.* $E_{photoanode}(j_{op}) = E_{photocathode}(j_{op})$ at an operating current density of j_{op}.

Similarly, the operating point of the tandem absorber + electrocatalyst PEC configuration is the intersection (red point) between the current density–voltage (*J–V*) behavior of a tandem light absorber (green curve in Fig. 2b) and the *J–V* behavior of a combined electrochemical load (blue curve in Fig. 2b). The electrochemical load curve includes the thermodynamic potential for water splitting, the polarization curves of both the HER and OER catalysts, and a linear *J–V* relationship to account for the solution resistance. The balance between the operating voltage, V_{op}, the thermodynamic potential for water splitting, the overpotentials of HER and OER catalysts, and the solution resistance loss at the operating photocurrent density, j_{op} is given by:

$$V_{op}(j_{op}) = 1.23\ V + |\eta_{HER}(j_{op})| + \eta_{OER}(j_{op}) + j_{op}R \quad (3)$$

The operating point (V_{op},j_{op}) for the tandem absorber + electrocatalyst PEC configuration is shown as the red intersection in Fig. 2b. For both Configuration A and B, the solar-to-hydrogen (STH) efficiency limit is defined as:[11,18,19]

$$\eta_{STH} = \frac{1.23\ (V) \times j_{op}\ (mA\ cm^{-2})}{S\ (mW\ cm^{-2})} \quad (4)$$

where j_{op} is the operating photocurrent density (mA cm^{-2}) and *S* is the total incident solar irradiance (mW cm^{-2}).

For the PV + electrolyzer configuration, the STH efficiency is the solar-to-electricity efficiency of the PV component, η_{PV}, multiplied by the electrolyzer efficiency, $\eta_{electrolyzer}$:

$$\eta_{STH} = \eta_{PV} \times \eta_{electrolyzer} \quad (5)$$

In the following section, each component of the PEC system including the light absorber and the electrocatalysts will be modeled as current and voltage or potentials, so that the operating point can be solved for numerically.

III Modelling

A Shockley–Queisser limits of light absorbers

The ideal *J–V* characteristics of two-junction or two-component light absorbers, *e.g.* $V_{top}(j)$ and $V_{bottom}(j)$ or $V_{op}(j_{op})$, was determined by a detailed-balance calculation,[21] with the current density at an operating photovoltage obtained from the sum of the incident solar radiation (J_{ph}) and the thermal radiation (J_{th}) minus the radiative emission (J_{rad}):

$$J = J_{ph} + J_{th} - J_{rad} \quad (6)$$

The analytical expressions for J_{ph}, J_{th} and J_{rad} presented by Henry[23] were used, with the detailed equations described in the ESI.†

In Configuration A, the top photoanode absorbs short-wavelength light, while the bottom photocathode absorbs long-wavelength light in a complementary fashion. In Configuration B, the tandem light absorber consists of serially connected top and bottom junctions, and the *J–V* characteristics can be calculated numerically by addition of the photovoltages of each junction at a given photocurrent density. In both configurations, radiative coupling between the top and bottom junctions was considered, wherein the radiative emission from the top junction entered the bottom junction.[24] As shown in Fig. 2a, the dashed blue and green curves represent the ideal *J–V* properties

of 1.60 eV top and 0.95 eV bottom junctions, and the green curve in Fig. 2b represents the ideal *J–V* properties of a tandem light absorber of a 1.60/0.95 eV bandgap combination. For the PV + electrolyzer configuration, the energy-conversion efficiency of a two-junction solar cell is the governing parameter.

To differentiate between the various qualities of light absorbers, three types of fill factors (FFs) were assigned to the detailed-balance *J–V* behavior. This consideration was included explicitly because finite mobility, low collection length, low minority-carrier lifetimes, and non-radiative recombination losses of photogenerated carriers can reduce the fill factors in the *J–V* behavior of the light absorber.[25–29] From the fill factors measured for record efficiency solar cells,[30] FF = 0.85, 0.75, and 0.68 for (1) III–V and crystalline Si solar cells, (2) thin film II–VI (CdTe) and chalcopyrite (CuInGaSe) solar cells, and (3) amorphous Si(Ge), organic PV and dye-sensitized solar cells. The FF, or the shape, of light absorber *J–V* curves depends on the specific parameters of the materials and devices used in the PV component. To simplify the modeling, an effective series resistance, R_s, was introduced to adjust the *J–V* behavior to the three FF cases:

$$J = -J_0\left\{\exp\left[\frac{e(V - JR_s)}{AkT}\right] - 1\right\} + I_{ph} \quad (7)$$

where J_0 is the total recombination current density, A is the diode ideality factor, k is the Boltzmann's constant, T is the absolute temperature, and I_{ph} is the photocurrent density.

B Behaviour of electrocatalysts

The kinetics of the HER and OER electrocatalysts were modeled by Butler–Volmer expressions, respectively:

$$i_{HER} = i_{0,HER}\left[\exp\left(\frac{\alpha_{a,HER}F\eta_{HER}}{RT}\right) - \exp\left(-\frac{\alpha_{c,HER}F\eta_{HER}}{RT}\right)\right] \quad (8)$$

$$i_{OER} = i_{0,OER}\left[\exp\left(\frac{\alpha_{a,OER}F\eta_{OER}}{RT}\right) - \exp\left(-\frac{\alpha_{c,OER}F\eta_{OER}}{RT}\right)\right] \quad (9)$$

where i_{HER}, i_{OER} are current densities of the HER and OER catalysts, respectively, η_{HER}, η_{OER} are the overpotentials of the HER and OER catalysts that are driven cathodically and anodically ($\eta_{HER} < 0$, $\eta_{OER} > 0$), respectively, R is the molar gas constant and F is Faraday's constant. The quantities $i_{0,HER}$ and $i_{0,OER}$ are HER and OER exchange current densities, respectively, and $\alpha_{a,HER/OER}$ and $\alpha_{c,HER/OER}$ are the HER and OER anodic and cathodic transfer coefficients, respectively. Pt for a HER catalyst and RuO_2 for an OER catalyst represent state-of-the-art noble-metal catalysts, while NiMo alloy for the HER and NiFe oxide ($NiFeO_x$) for the OER represent state-of-the-art earth-abundant catalysts for these reactions. The electrocatalytic properties of RuO_2 have been used to represent the behavior of some of best-performing OER electrocatalysts, including IrO_2 and RuO_2, although RuO_2 itself has limited stability under acidic conditions. NiMo + $NiFeO_x$ is only stable under alkaline conditions (pH = 14). The catalyst properties are listed in Table 1.

IV Results and discussion

Based on the theory and modeling, the STH efficiency limits were calculated numerically for each configuration. A matrix of STH efficiency values was generated for all of the band gap combinations of interest, with ranges of 1.3–2.4 eV for the top junction and 0.65–1.3 eV for the bottom junction, at a resolution of 0.05 eV and 0.025 eV for the top and the bottom junctions, respectively. The STH efficiency limits are presented as a contour plot, with the vertical and horizontal axes indicating the top and bottom junctions, respectively, of the light absorbers. As shown in Fig. 3–6, iso-efficiency curves were plotted by connecting the points of identical STH efficiencies in each configuration. Photovoltaic efficiencies of tandem solar cells have been presented previously in a similar format.[35,36] Note that the STH efficiencies are proportional to the operating current density in an integrated PEC system, under 1 Sun and standard conditions.

A STH efficiency and band gap combinations with noble-metal electrocatalysts

Fig. 3a and b show mutually identical STH efficiency contour plots for the photocathode + photoanode PEC configuration and for the tandem absorber + electrocatalysts PEC configuration. Pt + RuO_2 electrocatalysts, a fill factor of 0.85, and a solution resistance of 5 ohm cm^{-2} were used to represent an optimized design[17] for the PEC system. Both configurations exhibited a maximum STH efficiency of 29.7% at a band gap combination of 1.60 eV/0.95 eV. Achieving STH efficiencies of >25% requires band gap combinations in the range of 1.65–1.8 eV/0.95–1.15 eV.

Three regions with different contour lines were observed as a result of the calculations. The contour lines for top-junction band gaps of 1.95–2.30 eV are horizontal because the photocurrents of the top junction limited the overall photocurrents. At the lower left corner of the plots in Fig. 3a and b, the STH efficiency limit for any band gap combination is fundamentally restricted by the photovoltage provided by the light absorber, and the operating photocurrent density is well below its short-circuit photocurrent density. At the lower right corner, the STH

Table 1 Parameters for the electrochemical kinetics of HER and OER catalysts used

HER catalysts				OER catalysts			
Materials	Current density/overpotential	Tafel slope	Ref.	Materials	Current density/overpotential	Tafel slope	Ref.
Pt	55 mV/10 mA cm^{-2}	30 mV dec^{-1}	31	RuO_2	240 mV/10 mA cm^{-2}	37 mV dec^{-1}	32
Ni–Mo	75 mV/10 mA cm^{-2}	40 mV dec^{-1}	33	$NiFeO_x$	280 mV/10 mA cm^{-2}	40 mV dec^{-1}	34

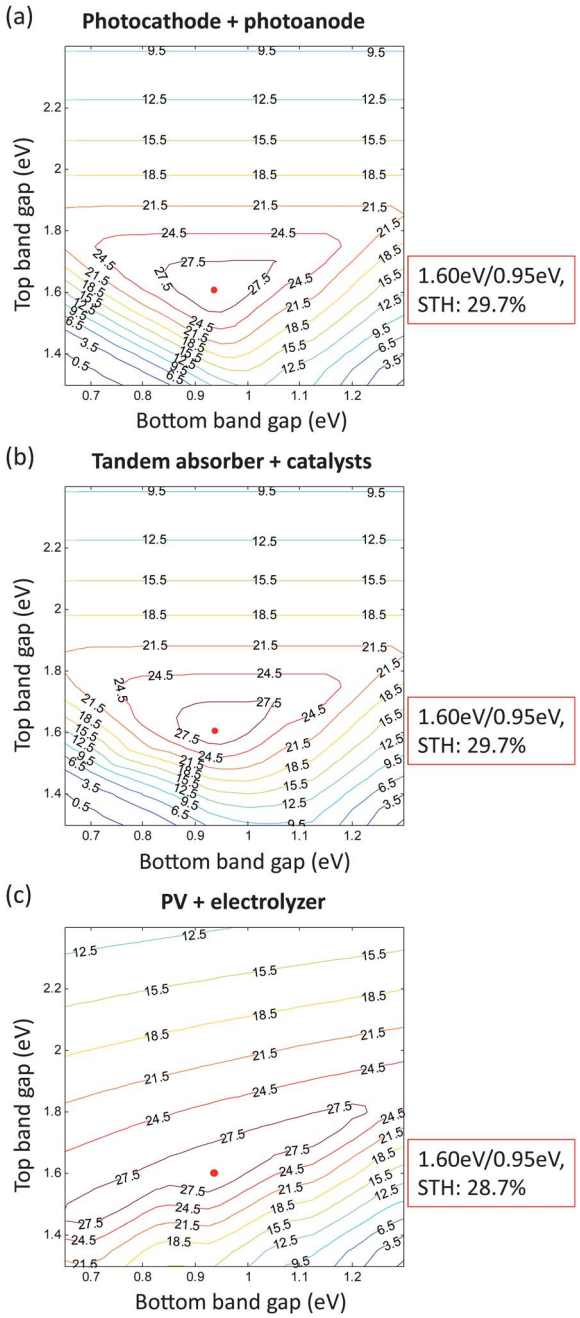

Fig. 3 Iso-efficiency plots showing the STH efficiency limits for (a) a photocathode + photoanode PEC, (b) a tandem absorber + electrocatalyst PEC, and (c) a two-junction PV + electrolyzer. In (a) and (b), Pt and RuO_2 were chosen as the HER and OER catalysts, the light absorber had FF = 0.85, and the solution resistance was 5 ohm cm^{-2}. In (c), the electrolyzer efficiency was taken to be 73%.

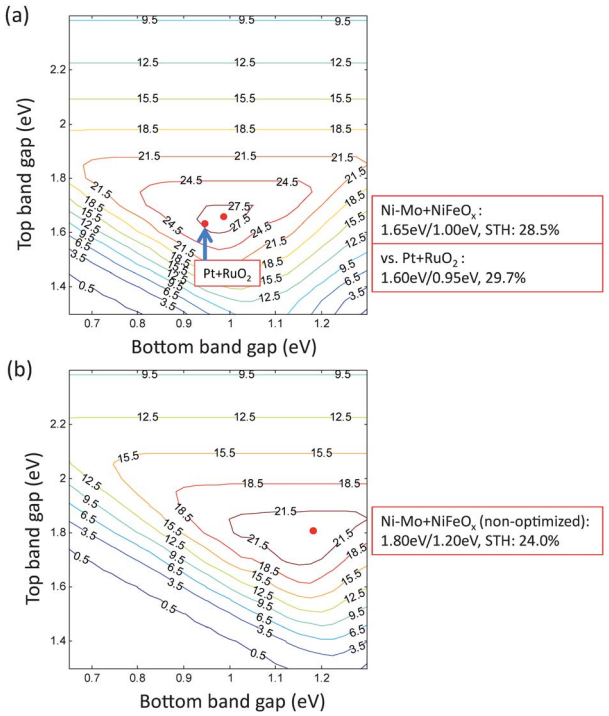

Fig. 4 Iso-efficiency plots of STH efficiency limits with earth-abundant catalysts, (a) Ni–Mo HER and $NiFeO_x$ OER electrocatalysts with a 280 mV overpotential at 10 mA cm^{-2}, and (b) Ni–Mo HER and non-optimized OER catalysts with a 560 mV overpotential at 10 mA cm^{-2}. The maximum STH efficiency limit for the case of the Pt and RuO_2 catalysts is labeled in Fig. 5a, for comparison. The light absorbers had FF = 0.85, and the solution resistance was 5 ohm cm^{-2}.

efficiency limit for any band gap combination drops quickly as the bottom-junction band gap decreases and approaches the top-junction band gap. This behavior occurs because the top junction shadows the bottom junction and limits the total photocurrent density of the tandem.

As discussed in the theory section, the principles for determining the STH efficiency limits are mathematically identical for both systems, which resulted in the identical plots shown in Fig. 3 for the different configurations. Therefore, all of the following calculations will only focus on the photocathode + photoanode PEC configuration. The negligible variation in the efficiency values between the two different configurations is due to round-off errors.

We first investigated the maximum STH efficiency possible for an integrated PEC water-splitting system. Under the Air Mass (AM) 1.5 solar spectrum at 1 Sun, the maximum STH efficiency is ~31.1%, at which point the STH efficiency is fundamentally limited by the maximum photocurrent density possible from a two-component or two-junction light absorber. This STH efficiency value corresponds to a matching photocurrent density of 25.3 mA cm^{-2}, at which point a 1.65 eV/0.95 eV tandem light absorber can drive the Pt + RuO_2 electrocatalysts as well as a solution resistance of up to 0.1 ohm cm^{-2}.

The operating point depends on the interplay between the light absorbers and the kinetics of the HER and OER electrocatalysts as well as ion transport considerations. To achieve water splitting at maximum STH efficiencies, two requirements need to be met: (1) the band gap combinations of the light absorbers need to be chosen to ensure current matching, and (2) the photovoltages provided by those current-matched light absorbers are able to drive the electrochemical load at a current density equal to, or close to, the matching short-circuit photocurrent densities when operated in separate water-splitting half-reactions. In a well-designed PEC system, the optimal STH efficiency is usually limited by the operating photocurrent density when an operating photovoltage of 1.5–1.8 V is

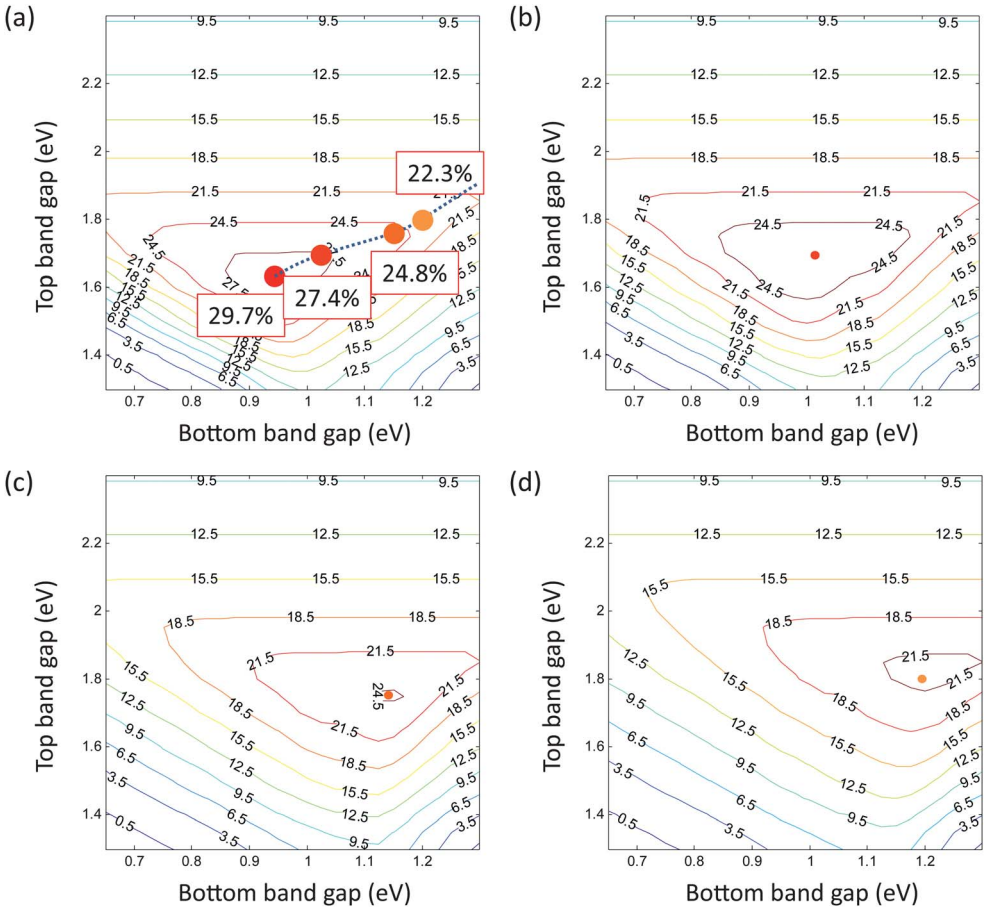

Fig. 5 Iso-efficiency plots of STH efficiency limits for a series of solution resistance values of: (a) 5, (b) 10, (c) 20, and (d) 30 ohm cm^{-2}. The dots in (a) represent the maximum STH efficiencies for $R = 5$, 10, 20, and 30 ohm cm^{-2}, with the traces varying as a function of the solution resistance value labeled as the dashed line. Pt and RuO_2 were chosen as HER and OER catalysts, respectively, and the light absorber had a FF = 0.85.

achieved.[12,13,15,16] In this case, improving the catalyst performance, increasing the catalyst loading, or decreasing the solution resistances will not improve the STH efficiency further.

Nonetheless, three additional factors need to be considered for the STH efficiency limits, and will reduce efficiency values below the ideal limit of 31.1%: (1) overpotentials of the HER and/or OER catalysts, (2) resistance losses of the solution electrolyte, and (3) decreasing FFs reflected in the *J–V* behavior of the light absorbers. In any case or all together, the photovoltage provided by the light absorber may fail to meet the voltage required to drive the combined electrochemical loads, and the STH efficiency limits then would need to be revisited.

B Effect of earth-abundant electrocatalysts

Fig. 4 indicates the STH efficiency limits for various choices of the HER and OER electrocatalysts. The use of earth-abundant catalysts, *e.g.* Ni–Mo alloy (NiMo, HER) and Ni–Fe oxide ($NiFeO_x$, OER), instead of noble-metal catalysts, *e.g.* Pt (HER) and RuO_2 (OER), results in additional catalyst overpotentials in the system. The maximum values of the STH efficiency limits were found to be 29.7% *vs.* 28.5% for Pt + RuO_2 catalysts *vs.* NiMo + $NiFeO_x$ catalysts, with light absorbers having FF = 0.85 and a solution resistance of 5 ohm cm^{-2}. The corresponding optimal band gap combinations were 1.60 eV/0.95 eV *vs.* 1.65 eV/0.98 eV. An OER catalyst with twice the overpotential of the $NiFeO_x$ catalyst, *e.g.* 560 mV at 10 mA cm^{-2}, was also considered, to represent non-optimized earth-abundant electrocatalysts (Fig. 4b). The optimal band gap combination was 1.80 eV/1.20 eV, with a maximum STH efficiency of 24.0%.

The choices of the HER and OER electrocatalysts can affect the STH efficiency limit significantly. When the photovoltage of the light absorbers at the power point cannot meet increasingly large catalyst overpotentials, the catalyst performance will limit the STH efficiencies. In Fig. 4a *vs.* b, the optimal band gap combination shifted to 1.80 eV/1.20 eV to provide the required photovoltage, and the STH efficiency value dropped from 28.5% to 24.0% due to insufficient absorption of solar spectrum at such a band gap combination. The 1.80 eV/1.20 eV bandgap tandem structure will accommodate a wide range of overpotentials, but as the overpotentials decrease at a given current density, different combinations of bandgaps will be optimal, and the corresponding optimal STH efficiency will increase. On the other hand, when the overpotentials of earth-abundant catalysts are comparable to those of the Pt + RuO_2 noble catalysts, the STH efficiency for the earth-abundant catalysts was

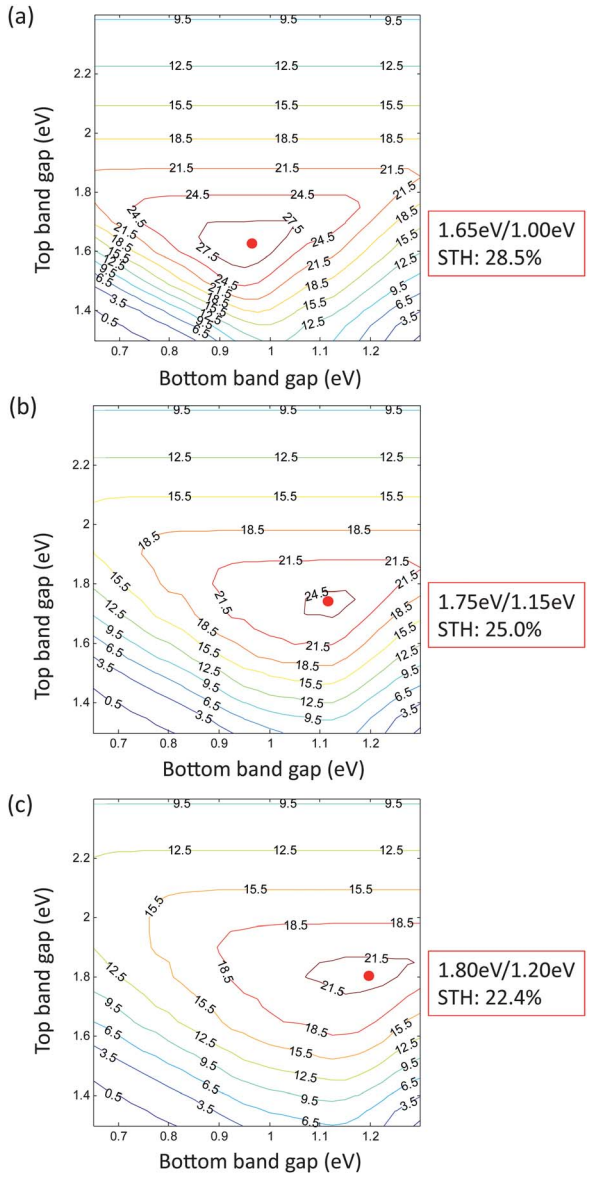

Fig. 6 Iso-efficiency plots of the STH efficiency limits for a series of light absorber fill-factors (FFs), (a) FF = 0.85, (b) FF = 0.75, and (c) FF = 0.68. State-of-the-art earth-abundant catalysts, such as NiMo and $NiFeO_x$, were chosen as the HER and OER catalysts, respectively, and the solution resistance was 5 ohm cm^{-2}.

only reduced to 28.7%, and the optimal band gap combinations only shifted slightly, from 1.65 eV/0.95 eV to 1.65 eV/0.98 eV. In other words, when the band gap combinations provided enough photovoltage, the improvement of the electrocatalysis does not improve the overall STH efficiency. For an integrated PEC system that operates at current densities of 10–20 mA cm^{-2}, replacement of noble-metal catalysts with earth-abundant catalysts is especially appealing. Regardless, more active earth-abundant catalysts are still desirable, because the catalyst loading can be reduced, mitigating the parasitic optical absorption by the catalyst particles. Furthermore, proper design is also necessary to prevent photocurrent crowding to a small portion of the catalyst,[17] so that the low overpotential catalyst properties can be effectively utilized in the system as a whole.

Although a top-junction band gap of >1.9 eV limits the overall photocurrents, the photovoltages provided by the light absorber can be high enough to enable the use of high overpotential electrocatalysts. The horizontal contour lines in Fig. 4a and b showed identical STH efficiencies, even when non-optimized OER catalysts having a 560 mV overpotential at 10 mA cm^{-2} were considered. In this case, STH efficiencies of 10–20% are still possible through efficient optical absorption and carrier collection, although the top junction limits the operating current density.

C Effects of solution resistance

Solution resistances of 5, 10, 20, and 30 ohm cm^{-2} were chosen for the integrated PEC system, which also contained light absorbers having FF = 0.85, Pt as the HER catalyst, and RuO_2 as the OER catalyst. Simulations of actual systems have shown that some geometries can produce Ohmic resistance drops of <100 mV for a photocurrent density of >20 mA cm^{-2}. Specifically, designs that produce an Ohmic resistance of 5 ohm cm^{-2} are accessible experimentally in integrated PEC systems, through suitable choice of the system geometry and with appropriate specification of the dimensions of the system components.[17] The resistive loss due to ion transport through ion-selective membranes, *e.g.* protons through Nafion®, have been neglected in this study, being small relative to the solution Ohmic resistances in a variety of optimized prototype designs.[17] As shown in Fig. 5a, the maximum STH efficiency was 29.7% for 5 ohm cm^{-2}, 27.4% for 10 ohm cm^{-2}, 24.8% for 20 ohm cm^{-2}, and 22.3% for 30 ohm. The corresponding optimal band gap combinations were 1.60 eV/0.95 eV, 1.70 eV/1.03 eV, 1.75 eV/1.15 eV, and 1.80 eV/1.20 eV.

As the solution resistance increased, the STH efficiency limit for a fixed band gap combination either stayed constant or decreased, resulting in the iso-efficiency plots of Fig. 4a–d. In addition, the distances between the iso-efficiency lines in these plots expanded with increased solution resistance, suggesting that when the operating photocurrent densities decreased substantially from the short-circuit values, the decreased STH efficiencies were less sensitive to the variation in the acceptable band gap combinations.

The STH efficiencies in an integrated PEC system are very sensitive to the solution resistance. As shown in Fig. 5, the Ohmic potential loss of the PEC system can reduce the STH efficiency and significantly shifts the optimal band gap combination for the light absorber. By increasing the solution resistance from 5 ohm to 45 ohm, the Ohmic potential losses can increase by as much as ~600 mV, while additional overpotential losses due to the use of earth-abundant catalysts are typically 60–340 mV at operating current densities of 10–20 mA cm^{-2}. The increased potential loss causes the operating point to decrease to a lower operating current density, further decreasing the STH efficiency. Therefore, emphasis should be placed on rational designs of integrated PEC systems, to minimize Ohmic potential losses. Good design is necessary because when the Ohmic potential loss is ~600 mV, even the best catalysts are not particularly useful in obtaining high overall STH system efficiencies.

D Effects of fill factor

Fig. 6 show a series of STH efficiency contour plots, for (a) FF = 0.85, (b) FF = 0.75, and (c) FF = 0.65. The change in the fill factor accounted for differences in the current–voltage behavior of the photoelectrode, in the absence of kinetic overpotentials. The STH efficiency limits were 28.5% for FF = 0.85, 25.0% for FF = 0.75, and 22.4% for FF = 0.68. The corresponding band gap combinations were 1.65 eV/0.98 eV, 1.75 eV/1.13 eV, and 1.80 eV/1.20 eV.

The STH efficiencies are also very sensitive to the shape of the *J–V* curves of the individual light absorbers. Decreasing the FF reduces the photovoltage produced by the light absorbers at the maximum power point. This behavior effectively reduces the current densities at the intersection point of the behavior of the two isolated light absorbers, in a fashion similar to the effects of varying the solution resistance.

The results above imply that the requirements on the performance and quality of the light absorbers are high: high FF (0.75–0.85), matching current density, and sufficient voltage at the optimal band gap combination. Band gap combinations of 1.65–1.80 eV/1.12 eV are practical. Si (1.12 eV) photocathodes with Pt[37,38] and NiMo[39,40] catalysts have been demonstrated with efficiencies approaching their bulk recombination limit. Substantial efforts should be devoted to the search for top-junction materials having a 1.65–1.8 eV band gap, which is current-matched to the bottom Si photoelectrodes in such a system. Furthermore, the photovoltages provided by the 1.65–1.8 eV/1.12 eV bandgap combination can accommodate additional overpotentials that are characteristic of many HER and OER catalysts, thus enabling the use of earth-abundant catalysts that operate at photocurrent densities of 10–20 mA cm^{-2} while still offering the opportunity for high maximum STH efficiencies for the system as a whole.

E Comparison to PV + electrolyzer

Dark electrolysis powered by PVs operates differently from an integrated PEC system in that the PV component and the electrolyzer each operate independently. An electrolyzer is optimized under its specific operating conditions, with an efficiency of 70–75%, and operates optimally at a current density of ~1 A cm^{-2} at a temperature of 70–80 °C (the PV component is not at this temperature).[41–44] The heat generated from the electrolysis process can be used to keep the unit running at the designed temperature of 70–80 °C.

As shown in Fig. 3c, the two-junction PV + electrolyzer configuration gives a maximum STH efficiency of 28.7% at a band gap combination of 1.60 eV/0.95 eV, assuming that the efficiency of the electrolyzer is 73%. These values are comparable to those of an integrated PEC system, however, fundamental differences exist between the two different types of system configurations. In an integrated PEC system, the optimal band gap combination depends on the specific design/operation parameters of the integrated PEC system, namely on the choices of the HER and OER catalysts and on the solution resistance. In a PV + electrolyzer configuration, the PV and the electrolyzer are optimized separately: the optimal PV efficiency is ~41%, at a 1.65 eV/0.95 eV band gap combination, regardless of the electrolyzer characteristics. In fact, the PV components are not necessarily limited to a two-junction tandem. For example, triple-junction III–V solar cells have achieved a PV efficiency of 43.5%.[30] Such a PV component operating with an electrolyzer of 73% efficiency will give a STH efficiency of 43.5% × 73% = 31.8%.

However, the output voltage and current of the PV component has to match with the input voltage and current of the electrolyzer, at least at one specific time of day. In addition to voltage regulators, specific wiring schemes can be used for the input–output matching. A bipolar alkaline electrolyzer can achieve an optimal efficiency of 73% by serially connecting a set of membrane-electrode assemblies to run at a multiplied input voltage and a reduced current density of each assembly.[43] For example, assuming that a 73% efficient bipolar electrolyzer unit requires an input voltage of 9 V and an input current density of 0.1 A cm^{-2}, and assuming that the output voltage and current density of the PV cell is 1.8 V and 20 mA cm^{-2}, a module of five serially connected PV cells can provide an output voltage of 9 V and can therefore be directly connected to the input of the electrolyzer. A PV area of 0.25 m^2 can match the input current of such an electrolyzer unit of 10 cm × 10 cm in size. When the PV area doubles, the number of electrolyzers will also double. Therefore, a roof of 25 m^2 in area would need 100 such 9 V electrolyzer units operating simultaneously. With such a wiring scheme, the STH efficiency of the PV + electrolyzer configuration is simply the photovoltaic efficiency of a tandem PV component multiplied by the electrolyzer efficiency.

V Conclusions and perspective

The solar-to-hydrogen efficiency reflects the interplay of all of the components of an integrated photoelectrochemical system, and the operating parameter of each component influences the overall solar-to-hydrogen (STH) efficiency. The maximum STH efficiency for an integrated PEC system is ~31.1% at 1 Sun, with the corresponding STH efficiency limited by the maximum photocurrent density possible from the two-component or two-junction light absorber. An operating current density of 10–20 mA cm^{-2} enables the use of earth-abundant catalysts while achieving comparable STH efficiencies to those obtainable by use of noble-metal electrocatalysts. The fill factor of the light absorber current–voltage behavior and the Ohmic resistance of the electrolyte solution also play key roles in determining the optimal STH efficiency and the corresponding band gap combination. Practically, light-absorbing materials having a 1.6–1.8 eV band gap that are integrated with Si are promising candidates for tandem-based light absorber structures for water splitting at >25% efficiencies.

In actuality, the carrier generation, carrier transport, catalyst turnover, and ionic transport are all spatially distributed. Future studies extending such modeling to 3-D will be important for evaluating and optimizing specific geometric system designs at both the device and system levels. In addition, the effects of multi-exciton generation[45] and solar concentration coupled with carrier multiplication[46] should be considered with respect to the design of specific system architectures for solar-driven

water splitting. Similarly, the operating principles and efficiency limits of solar-fuel reactors based on combined solar-thermal-electrochemical production (STEP) cycles should be evaluated in detail as well.[47]

Acknowledgements

This work was supported through the Office of Science of the U.S. Department of Energy under Award no. DE-SC0004993 to the Joint Center for Artificial Photosynthesis, a DOE Energy Innovation Hub.

Notes and references

1 A. Fujishima and K. Honda, *Nature*, 1972, **238**, 37–38.
2 A. Kumar, P. G. Santangelo and N. S. Lewis, *J. Phys. Chem.*, 1992, **96**, 834–842.
3 W. J. Youngblood, S.-H. A. Lee, Y. Kobayashi, E. A. Hernandez-Pagan, P. G. Hoertz, T. A. Moore, A. L. Moore, D. Gust and T. E. Mallouk, *J. Am. Chem. Soc.*, 2009, **131**, 926–927.
4 A. J. Nozik, *Appl. Phys. Lett.*, 1976, **29**, 150.
5 A. J. Nozik, *Appl. Phys. Lett.*, 1977, **30**, 567.
6 K. Sayama, K. Mukasa and R. Abe, *Chem. Commun.*, 2001, 2416–2417.
7 R. Abe, T. Takata, H. Sugihara and K. Domen, *Chem. Commun.*, 2005, 3829–3831.
8 R. Abe, K. Shinmei, K. Hara and B. Ohtani, *Chem. Commun.*, 2009, 3577–3579.
9 J. Brillet, J. Yum, M. Cornuz, T. Hisatomi, R. Solarska, J. Augustynski, M. Graetzel and K. Sivula, *Nat. Photonics*, 2012, **6**, 2–6.
10 R. E. Blankenship, D. M. Tiede, J. Barber, G. W. Brudvig, G. Fleming, M. Ghirardi, M. R. Gunner, W. Junge, D. M. Kramer, A. Melis, T. A. Moore, C. C. Moser, D. G. Nocera, A. J. Nozik, D. R. Ort, W. W. Parson, R. C. Prince and R. T. Sayre, *Science*, 2011, **332**, 805–809.
11 J. R. Bolton, S. J. Strickler and J. S. Connolly, *Nature*, 1985, **316**, 495–500.
12 O. Khaselev, *Science*, 1998, **280**, 425–427.
13 S. Licht, *Int. J. Hydrogen Energy*, 2001, **26**, 653–659.
14 G. Peharz, F. Dimroth and U. Wittstadt, *Int. J. Hydrogen Energy*, 2007, **32**, 3248–3252.
15 R. E. Rocheleau, E. L. Miller and A. Misra, *Energy Fuels*, 1998, **12**, 3–10.
16 S. Y. Reece, J. A. Hamel, K. Sung, T. D. Jarvi, A. J. Esswein, J. J. H. Pijpers and D. G. Nocera, *Science*, 2011, **334**, 645–648.
17 S. Haussener, C. Xiang, J. M. Spurgeon, S. Ardo, N. S. Lewis and A. Z. Weber, *Energy Environ. Sci.*, 2012, 9922–9935.
18 M. G. Walter, E. L. Warren, J. R. McKone, S. W. Boettcher, Q. Mi, E. a. Santori and N. S. Lewis, *Chem. Rev.*, 2010, **110**, 6446–6473.
19 Z. Chen, T. F. Jaramillo, T. G. Deutsch, A. Kleiman-Shwarsctein, A. J. Forman, N. Gaillard, R. Garland, K. Takanabe, C. Heske, M. Sunkara, E. W. McFarland, K. Domen, E. L. Miller, J. A. Turner and H. N. Dinh, *J. Mater. Res.*, 2011, **25**, 3–16.
20 (*a*) Y. Surendranath, D. K. Bediako and D. G. Nocera, *Proc. Natl. Acad. Sci. U. S. A.*, 2012, **109**, 15617–15621; (*b*) L. C. Seitz and T. F. Jaramillo, private communication.
21 W. Shockley and H. J. Queisser, *J. Appl. Phys.*, 1961, **32**, 510.
22 A. J. Nozik, *Appl. Phys. Lett.*, 1977, **30**, 567.
23 C. H. Henry, *J. Appl. Phys.*, 1980, **51**, 4494.
24 A. Martí and G. L. Araújo, *Sol. Energy Mater. Sol. Cells*, 1996, **43**, 203–222.
25 J. Mattheis, J. Werner and U. Rau, *Phys. Rev. B: Condens. Matter Mater. Phys.*, 2008, **77**, 1–13.
26 B. W. Faughnan and R. S. Crandall, *Appl. Phys. Lett.*, 1984, **44**, 537.
27 D. Macdonald and A. Cuevas, *Prog. Photovoltaics*, 2000, 252–264.
28 L. M. Andersson, C. Müller, B. H. Badada, F. Zhang, U. Würfel and O. Inganäs, *J. Appl. Phys.*, 2011, **110**, 024509.
29 Y. Zhang, X.-D. Dang, C. Kim and T.-Q. Nguyen, *Adv. Energy Mater.*, 2011, **1**, 610–617.
30 M. A. Green, K. Emery, Y. Hishikawa, W. Warta and E. D. Dunlop, *Prog. Photovoltaics*, 2012, **20**, 12–20.
31 S. Trasatti, *J. Electroanal. Chem. Interfacial Electrochem.*, 1972, **39**, 163–184.
32 G. Lodi, E. Sivieri, A. Battisti and S. Trasatti, *J. Appl. Electrochem.*, 1978, **8**, 135–143.
33 D. Brown, M. Mahmood, A. Turner, S. Hall and P. Fogarty, *Int. J. Hydrogen Energy*, 1982, **7**, 405–410.
34 J. Landon, E. Demeter, N. İnoğlu, C. Keturakis, I. E. Wachs, R. Vasić, A. I. Frenkel and J. R. Kitchin, *ACS Catal.*, 2012, **2**, 1793–1801; M. W. Louie, private communication.
35 S. R. Kurtz, P. Faine and J. M. Olson, *J. Appl. Phys.*, 1990, **68**, 1890.
36 T. J. Coutts, J. S. Ward, D. L. Young, K. A. Emery, T. A. Gessert and R. Noufi, *Prog. Photovoltaics*, 2003, **11**, 359–375.
37 S. W. Boettcher, E. L. Warren, M. C. Putnam, E. A. Santori, D. Turner-Evans, M. D. Kelzenberg, M. G. Walter, J. R. McKone, B. S. Brunschwig, H. A. Atwater and N. S. Lewis, *J. Am. Chem. Soc.*, 2011, **133**, 1216–1219.
38 T. Stempel, M. Aggour, K. Skorupska, A. Muñoz and H.-J. Lewerenz, *Electrochem. Commun.*, 2008, **10**, 1184–1186.
39 J. R. McKone, E. L. Warren, M. J. Bierman, S. W. Boettcher, B. S. Brunschwig, N. S. Lewis and H. B. Gray, *Energy Environ. Sci.*, 2011, **4**, 3573.
40 E. L. Warren, J. R. McKone, H. A. Atwater, H. B. Gray and N. S. Lewis, *Energy Environ. Sci.*, 2012, **5**, 9653.
41 A. F. Marshall, S. Sunde, M. Tsypkin and R. Tunold, *Int. J. Hydrogen Energy*, 2007, **32**, 2320–2324.
42 F. Barbir, *Sol. Energy*, 2005, **78**, 661–669.
43 J. Ivy, *Summary of Electrolytic Hydrogen Production: Milestone Completion Report*, National Renewable Energy Laboratory, Golden, CO, 2004.
44 J. Newman, P. G. Hoertz, C. A. Bonino and J. A. Trainham, *J. Electrochem. Soc.*, 2012, **159**, A1722–A1729.
45 M. C. Hanna and A. J. Nozik, *J. Appl. Phys.*, 2006, **100**, 074510.
46 M. C. Hanna, M. C. Beard and A. J. Nozik, *J. Phys. Chem. Lett.*, 2012, **3**, 2857–2862.
47 S. Licht, *Adv. Mater.*, 2011, **23**, 5592–5612.

